Materials Science in Semiconductor Processing 193 (2025) 109489

Contents lists available at ScienceDirect

Materials Science in Semiconductor Processing

journal homepage: www.elsevier.com/locate/mssp

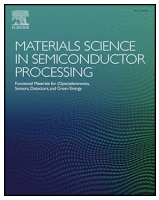

Toward characterization and assessment of MoS_2 fundamental device properties by photoluminescence

Thomas Nuytten *, Albert Minj, Stefanie Sergeant, Quentin Smets, Steven Brems, Pawan Kumar, Souvik Ghosh, Tom Schram, Sreetama Banerjee, Anastasiia Kruv, Dennis van Dorp, Benjamin Groven, Pierre Morin

Imec, Kapeldreef 75, B-3001, Leuven, Belgium

ARTICLE INFO

Keywords:
Metrology
Photoluminescence
Nano-electronics
Characterization
Semiconductor technology

ABSTRACT

The continuous expansion of two-dimensional materials research since the first developments of over 15 years ago has enabled tremendous progress in the fundamental understanding of their properties and behavior. The promises held by these materials to facilitate scaling beyond silicon-based device architectures are still valid, but the manufacturability and integration with silicon technology remain challenging. On the metrology side, characterization of the device channel and assessment of the expected performance is lacking, at least in a fully non-destructive and process line-compatible implementation. The current paper demonstrates a clear correlation between metrics associated with the transistor performance on one hand, and parameters from photoluminescence spectra on the other. The concept is demonstrated on state-of-the-art 300 mm process MoS_2 devices, without the need for specific measurement conditions or sample preparation. Being truly non-contact and relatively fast, this analysis provides the community with a potential route toward non-invasive material quality assessment, applicable at several stages of the process and with a direct connection to device performance.

1. Introduction

The introduction of 2D materials in high-volume manufacturing to overcome scaling limits associated with conventional semiconductor materials becomes increasingly tangible as their use appears on recent technical roadmaps, further accelerated by the rapid advances in the manufacturability and integration approaches for these exploratory materials [1–4]. While impressive progress in device fabrication has been made, the precise path toward reliable material characterization that is process-line compatible and provides an unambiguous assessment of the material quality and expected device characteristics remains unclear. Encouraging results have been obtained using in-plane X-ray diffraction and sub-micrometer four-point probe measurements [5,6], but most reports aim to develop photoluminescence (PL) into a defectivity measurement for transition metal dichalcogenides (TMDCs) [7–9]. In general the PL response of 2D materials is strongly dependent on a wide variety of parameters such as local doping [10–13], defectivity [14], temperature [15,16] and strain [17]. Low-temperature PL is particularly promising through a defect-assisted recombination that emerges at cryogenic temperatures [18], and holds the promise to be quantitatively linked to (intrinsic) material defectivity, at the cost of being only applicable at liquid nitrogen temperatures or below, making the technique unsuited for inline application. On the other hand, detailed analysis of the spectral components in the room-temperature PL with or without back-gate bias enable the assessment of critical material parameters like trion binding energy [11–13] and charge carrier density [19,20]. While providing unexplored fundamental insight, a direct correlation between biased or unbiased PL and the ultimate transistor performance of a functional device (as extracted from electrical transport measurements on the semiconductor device) remains unexplored. Meanwhile it has become evident that substrate, device contact and ambient interactions and interfaces have a critical impact on the material's properties, if not being absolutely dominant for device performance [21,22].

In the present study we correlate this device performance with PL measurements both at low and ambient temperatures in an effort to provide guidance for the use of PL as a non-destructive, high-volume manufacturing (HVM)-compatible pre-screening metrology for 2D

This article is part of a special issue entitled: 2D Materials published in Materials Science in Semiconductor Processing.

* Corresponding author.
E-mail address: thomas.nuytten@imec.be (T. Nuytten).

https://doi.org/10.1016/j.mssp.2025.109489
Received 20 December 2024; Received in revised form 27 February 2025; Accepted 17 March 2025
Available online 25 March 2025

materials-based nano-electronic devices.

2. Materials and methods

The μm-sized MoS_2 FETs considered for PL were selected from a full wafer that was fabricated using a 300 mm integration platform and representative examples are shown in Fig. 1(a–c). The MoS_2 was formed by metal-organic chemical vapour deposition (MOCVD) on 2-inch sapphire substrates, resulting in a closed monolayer with some bilayer regions. The MoS_2 was transferred using rigid carriers to 300 mm Si wafers with a 50 nm SiO_2 oxide layer serving as the back-gate stack. Polymer residues from transfer were removed by a solvent strip and a remote H plasma clean. Subsequently, the MoS_2 was capped by 1 nm AlO_x and 10 nm HfO_2 and encapsulated in SiO_2. Side contacts were formed with a stack of Ti/TiN/W and a damascene process (M0 level), followed by the via (TiN/W) and M1 (TiN/W) metallization levels. The final thickness of the SiO_2 encapsulation is 270 nm. The devices considered for this study have a range of channel width W_{ch} = 1–75 μm and channel length L_{ch} = 1–32 μm. More details on the growth and processing of the MoS_2 devices can be found in Refs. [23,24]. Electrical measurements are performed on the back-gated devices, and the transfer characteristics of four selected devices are shown in Fig. 1(d–e). The threshold voltage of each device is extracted using the linear extrapolation method [V_{tLE}, see Fig. 1 (e)]. A trend is seen where smaller channel areas are affected more strongly by n-type doping, resulting in very negative V_{tLE} and lack of turn-off in the applied gate bias sweep range. It is well known that AlO_x deposited on MoS_2 can cause n-type doping [25,26], but it is unusual to have a dependence on the size of the channel area. We investigate whether this stronger n-type doping for smaller channel areas can be captured by PL. For the PL measurements on uncapped MoS_2, separate samples were created with similar MoS_2 transferred to Si/SiO_2 coupons using the thermal release tape method. It is important to analyze these batches of samples independently, since the capping layer itself is known to induce material-specific doping which in turn influences the PL response [26,27].

PL spectra were obtained using a Horiba Scientific LabRAM HR spectrometer using excitation at 532 nm through a 100X 0.9NA objective resulting in a spot size of about 1 μm with a laser power density at the sample of about 0.3 $mW/\mu m^2$. The scattered light was collected through the same objective, dispersed using a 300 g/mm grating followed by an OE CCD, with a typical integration time of 10 s per window and the resulting spectra were analyzed using Fityk [28] for extraction of peak parameters. The cryogenic PL measurements were carried out using a Linkam THMS600 temperature and environmental control stage capable of reaching temperatures down to 77 K. For back-gated PL measurements, a top contact was established using Ag paste directly on the MoS_2 surface for adequate grounding.

3. Results and discussion

As an initial verification of the applicability, to our material system, of PL-based defectivity characterization methods as established in previous literature, one batch of uncapped samples was studied using low-temperature PL right after the transfer process. Fig. 2 (a) shows the normalized PL at 77 K using various back-gate voltages applied to the uncapped but transferred MoS_2 layers. The spectrum is composed of a convoluted main peak just below 2 eV originating from both negatively charged (trion, A^-) and neutral exciton (A) recombination at zero and low bias. In agreement with previous literature [18], a faint and broad signal X^D emerges at lower energy as the back-gate bias is made more negative. At around −30 V this feature starts to dominate the spectrum and may continue to do so until sample failure occurs due to dielectric breakdown of the back-gate stack at these relatively elevated voltages. The feature is due to defect-assisted recombination and has a strong dependency on the local charge density and dynamics. Simultaneously, we observe that as the back-gate bias is made more negative and the MoS_2 is depleted from electrons, the main recombination equilibrium is shifted toward the neutral exciton at the expense of trion recombination (see horizontal arrow in the figure with associated peak shift), which is in good agreement with previous literature and interpretation studying the lowering of trion binding energy with increasingly negative back-gate bias [11–13]. The altered local charge density affects the different recombination mechanisms differently, which now favors the defect-assisted recombination X^D, increasing its relative intensity. At strong negative bias and associated depletion of the channel region, the defect levels become partly unoccupied, increasing the probability for the levels to contribute to the radiative recombination, in contrast to the strong n-type doping present at zero bias. Since both the trion/exciton intensity ratio and the defect peak intensity depend on the local charge density, this provides an opportunity for quantitative defect characterization. It has been shown how the trion spectral weight can be used to directly calculate the electron density, provided that an unambiguous deconvolution of the trion and A exciton is possible [19,20]. Moreover, when the back-gate voltage is tuned such that the A^-/A intensity ratio is the same for the samples one wants to compare, then the X^D intensity can be used as a gauge for intrinsic defectivity in those samples [18].

It is important to emphasize that due to the carrier dynamics in these systems, the defect-assisted recombination only appears at liquid nitrogen temperatures (or even below) which greatly complicates the applicability of this assessment as a routine and fast quality control. Moreover, it is known that experimental and environmental conditions play a critical role in optical characterization of TMDC materials, with pronounced PL dependency on parameters like for instance excitation energy and/or power [9,19,20], temperature [13,16] and strain [17]. As a demonstration we carried out a through-exposure type of PL experiment where the room temperature PL is recorded over a time interval of

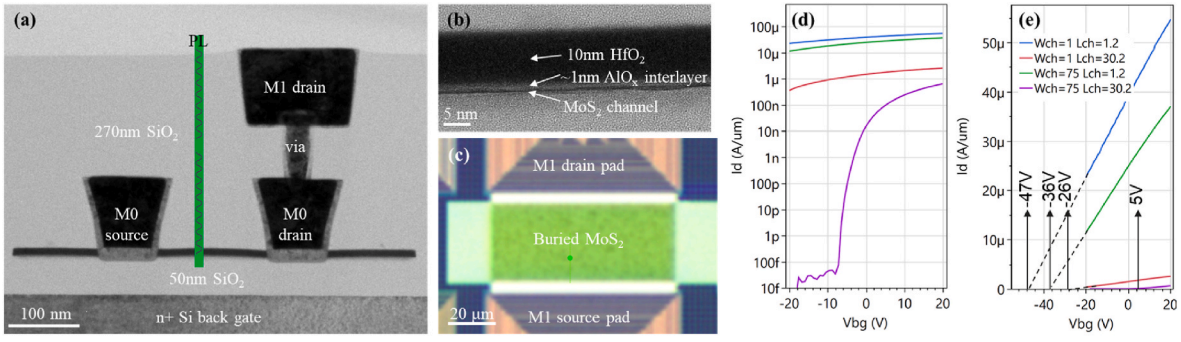

Fig. 1. (a) TEM of integrated device with buried MoS_2 channel. The green bar is a schematic representation of how the PL measurement probes through the oxide to reach the MoS_2. (b) Zoom-in on the stack with MoS_2/AlO_x interlayer/HfO_2 cap. (c) Optical image of device with larger W_{ch} = 75 μm and L_{ch} = 30.2 μm considered for PL. (d) Transfer characteristics in log-lin scale of four selected devices with different dimensions. (e) Transfer characteristics of those same devices in lin-lin scale demonstrating the V_{tLE} extraction method. (For interpretation of the references to colour in this figure legend, the reader is referred to the Web version of this article.)

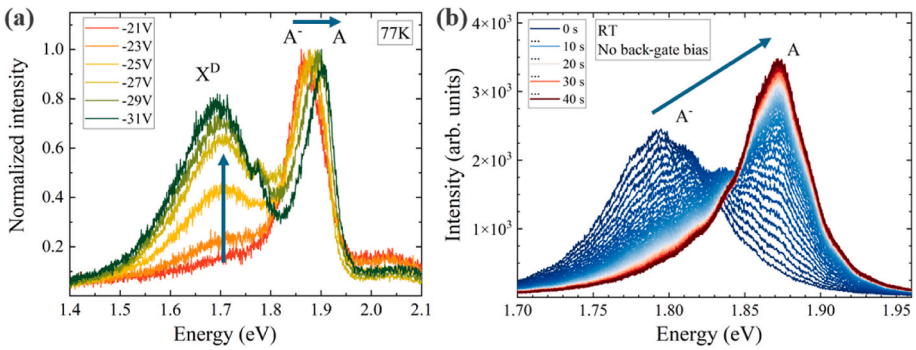

Fig. 2. (a) Back-gate bias-dependent PL at liquid nitrogen temperature (77 K) for a transferred, uncapped MoS_2 sample showing tunability of both the trion and neutral exciton recombinations, and the defect-assisted signal. (b) Time-dependent cascade of the 0.5 s integration time room temperature PL over a time interval of 40 s using a laser power density of 0.3 mW/μm^2 on the sample.

40 s with integration steps at 0.5 s under a continuous laser exposure of 0.3 mW/μm^2, which is a standard laser power density for PL and Raman experiments. It is shown in Fig. 2 (b) that during this relatively short time, the resulting spectrum is evolving in a rather dramatic way where we see a shift in intensity and peak position from a trion-dominated to a neutral exciton-dominated spectrum. It is hard to pinpoint the exact mechanism behind this evolution, which will probably be a combination of local heating and charge modification, as well as laser-assisted material degradation, given that the modifications are not universally reversible. This further emphasizes the need for a consistent measurement strategy and the importance of a preserving capping layer that will stabilize the samples throughout the measurement campaigns.

The uniformity of the integrated MoS_2 FETs was investigated through Raman and PL mapping experiments on large-area devices [Fig. 1 (c)], where a complete area of 10 × 10 μm was measured using a step size of 200 nm. This is much smaller than the laser spot size (~1 μm), but it can be seen from Fig. 3 that the resulting hyperspectral maps provide a good spatial resolution. In the representative Raman spectrum of panel (a) we observe the well-resolved characteristic E_{2g} and A_{1g} signals in addition to the Si background from the substrate. The PL spectrum [panel (e)] consists of the A^- and A convoluted contributions, in addition to a signal at higher energy related to the B exciton (not considered here). The inset panel (d) shows an optical micrograph of the selected region, where small features of higher contrast can be observed, indicative of bilayer regions. On these features, it is seen on panel (b) and (c) that the Raman intensity is higher for both characteristic peaks, while panel (f) shows that these locations correspond to a wider separation between the E_{2g} and A_{1g} signals. Finally, panel (g) shows that these features have a larger relative A^- contribution in the PL, which together with the Raman observations confirms that these are indeed bilayer islands on top of a monolayer closed layer, which is typical for the current crystal growth approach (see Refs. [23,24]).

For a first investigation into the link between PL parameters and electrical parameters, we select the four devices from Fig. 1(d–e) with a varying channel area and distinct differences in the extracted electrical parameters. Namely, a range of extracted V_{tLE} between about −50 and +5V is available and it can be seen from Fig. 4 (a) that correspondingly the PL signature at 77 K of these four devices is quite different. Generally, there is a convoluted trion/exciton recombination at around 1.9 eV and then a lower energy defect-assisted peak that varies greatly in intensity. In contrast to the strong dependence of the peak shape with the device dimensions, the signal is very uniform within each device. This

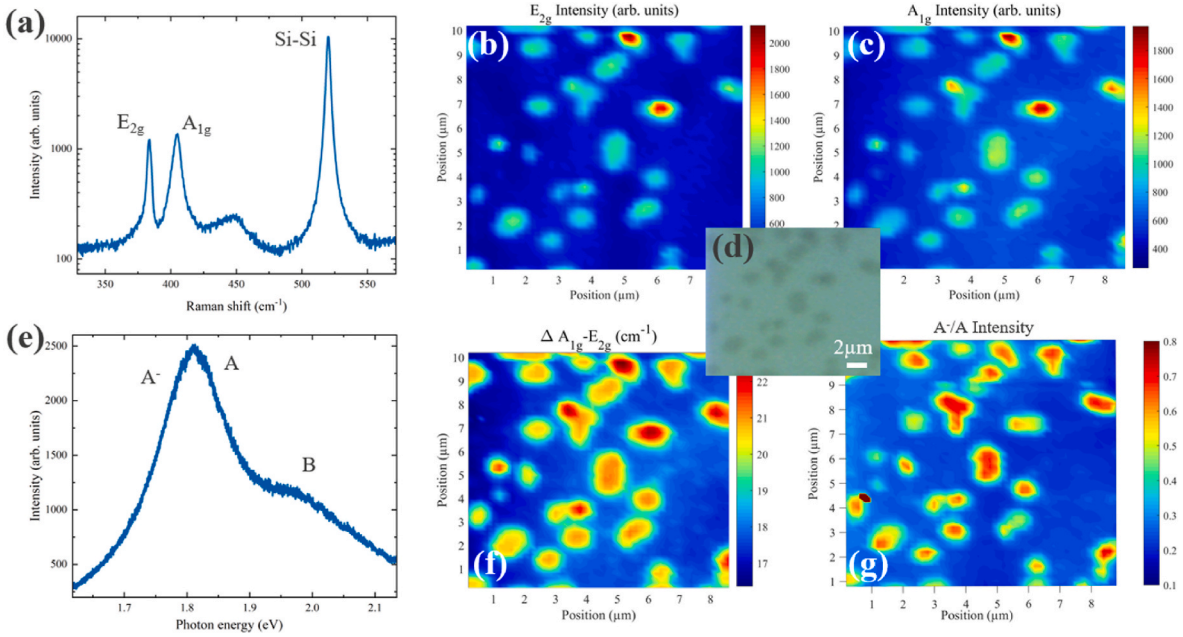

Fig. 3. Representative Raman (a) and PL (e) spectra for a 10 × 10 μm area of a capped MoS_2 device area. Analysis reveals a fully closed monolayer with isolated bilayer islands as evidenced from the E_{2g} (b) and A_{1g} (c) intensity, A_{1g} - E_{2g} peak separation (f) and trion to exciton intensity ratio (g). The inset (d) shows an optical micrograph of the studied region, where the shape and pattern of the bilayer islands can be recognized.

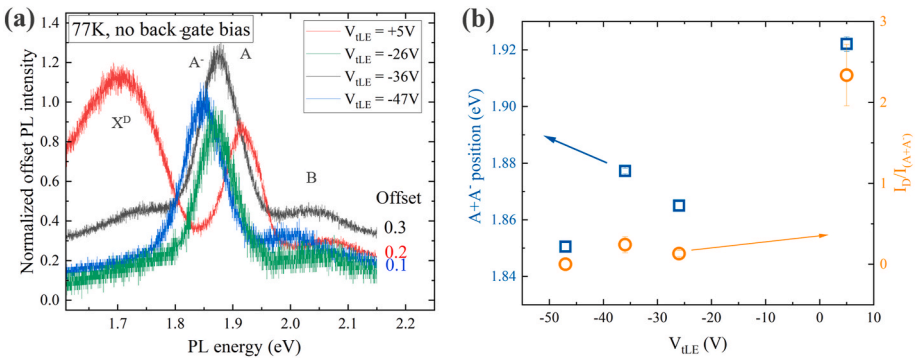

Fig. 4. (a) PL spectra at liquid nitrogen temperature for a selection of four devices with strongly different V_{tLE} (spectra are offset in intensity for clarity). (b) Fitted PL position (left) and defect to exciton intensity ratio (right) as a function of the threshold voltage.

stable trion-exciton intensity ratio points to uniform doping within the channel, despite the dependence on total channel area. As referred to before, it is possible to estimate the electron concentration *n* from the spectral weight of the trion component in the spectrum, which for our samples gives densities in the range between 0.2 and 7.2 × 10^{13} cm^{-2}, which is in line with earlier reports [11,19]. As expected there is a, albeit non-perfect, correlation between the calculated electron density derived from PL and the V_{tLE} obtained from the transport measurements, where globally a strongly negative V_{tLE} corresponds to a larger electron density. We note however that firstly, the PL here is recorded at cryogenic temperatures while the V_{tLE} is determined at room temperature. Secondly, and more importantly, the PL signature of the devices that we are considering is of that nature that an unambiguous spectral deconvolution of defect signal, trion, exciton and B exciton contribution is far from straightforward. The small binding energy of the trion (typically a few tens of meV) results in a closely convoluted A^- and A signal, and this is the main reason why we carry out the fitting by incorporating both the trion and exciton contribution, and we attempt to correlate that parameter with direct electrical measurements of the transistor behavior. The peak parameters can reliably be extracted from fitting several measurements on the same device, where a *single* Voigt profile was used to fit the convoluted A^- and A signals. Additionally, this approach allows to obtain a representative set of parameters for the PL which may cover both single and bilayer regions, which becomes evident only when assigning individual peak profiles for both contributions in the fitting [see Fig. 3 (g)]. In Fig. 4 (b) we can see that for both the intensity ratio between defect and exciton peak ($I_D/I_{(A + A^-)}$, right Y axis) and the PL peak position (left Y axis) a trend seems to appear as a function of the threshold voltage, which was obtained from transport measurements on the same devices. At large negative V_{tLE}, the device is strongly n-type, and the excess electrons give rise to an increased charged exciton contribution, shifting the main PL peak to lower energy. Conversely, a positive V_{tLE} indicates a depleted channel at zero bias, with strongly reduced trion/exciton emission and a higher intensity defect-related peak. Despite the fact that this data seems to confirm a direct link between the defect-related emission and the electrical parameters, the defect signal only appears for the device characterized by low electron concentration at zero bias (i.e. positive V_{tLE}), while it is absent for the other samples. Additionally, the requirement to work at cryogenic temperatures further impedes the application of this approach as a universal quality assessment. For the remainder of the study it is therefore worth focusing on the extracted peak position, which, as can be seen in Fig. 4 (b), presents a similar correlation to the threshold voltage.

To further illustrate that PL is an easy-to-use method that can predict electrical device parameters, we demonstrate good correlation on a larger sample set at room temperature spanning a similar range in extracted V_{tLE}, but importantly the characterization was carried out at room temperature again. The complete collection of PL spectra obtained from all devices is plotted in panel (a) of Fig. 5, which shows a much more uniform PL emission across devices compared to the situation at 77 K. The main recombination now appears around 1.8 eV as expected and is still characterized by a convoluted trion and neutral exciton emission, which are fitted simultaneously using a single Voigt profile, from which the peak parameters are extracted. Since no defect signal is present at room temperature, the analysis focuses on the PL peak position and it can be seen in Fig. 5 (b) that a similar dependence of the recombination energy on V_{tLE} is found, providing further evidence for a direct link between parameters extracted from room-temperature PL without further detailed deconvolution, and an electrical parameter obtained directly from transfer characteristics of the transistor device. The V_{tLE} is used as a metric for channel doping (to avoid contact-induced limitations that may affect devices of varying dimensions differently), while the overall PL peak position incorporates the relative distribution between charged and neutral recombination, which in turn is linked to the same carrier distribution inside the channel. A positive V_{tLE} in the absence of back-gate bias is indicative of low electron concentration in the channel, which in turn will lead to a larger exciton to trion ratio, and an effective shift to higher recombination energy of the convoluted PL peak. Note that this is the same trend that was observed at low temperatures (see Fig. 4), but is also fully consistent with the behavior in back-gated regime [Fig. 2 (a)]. Indeed a strongly negative back-gate bias depletes the channel of electrons, which again shifts the PL energy to higher energy. The correlation between those two parameters means that one can pre-assess future device performance from a fully non-invasive, inline-compatible and fast spectroscopy measurement, without the need for establishing electrical contacts.

4. Conclusion

In summary, the low- and room-temperature PL from functional MoS_2 devices was investigated in relation to their electrical performance. A complete dataset of devices with varying dimensions and electrical behavior was selected, where the linearly extrapolated V_{tLE} was used as a metric for local charge density, while the direct recombination PL peak position of the convoluted trion and neutral exciton was used as the spectroscopic signature carrying similar information of the local charge distribution. At 77 K, but also at room temperature, a direct link between the PL peak energy and the extracted V_{tLE} was observed, demonstrating the ability to obtain information on the electrical behavior of the channel material from a non-contact optical characterization method. As such, the current approach provides a path to non-destructive, optical material pre-screening for electrical performance assessment, with the potential to be applied in an HVM environment.

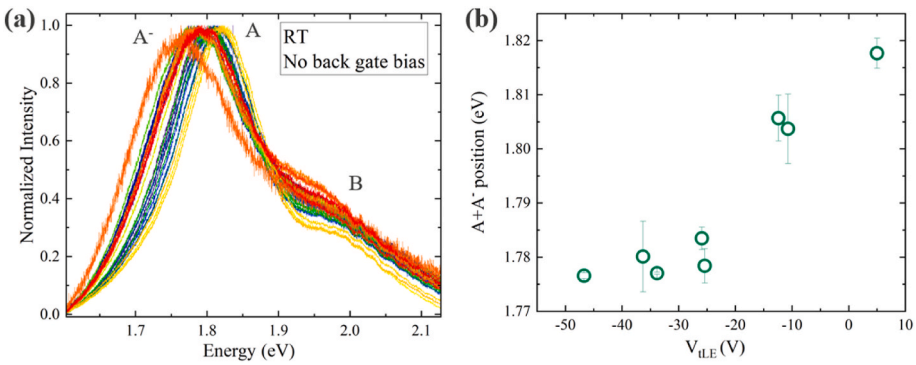

Fig. 5. (a) Normalized room temperature PL spectra for the complete collection of devices with varying electrical behavior as extracted from the transport measurements. (b) Fitted PL peak position as a function of the threshold voltage.

CRediT authorship contribution statement

Thomas Nuytten: Writing – original draft, Visualization, Validation, Supervision, Resources, Project administration, Methodology, Investigation, Formal analysis, Data curation, Conceptualization. **Albert Minj:** Methodology, Investigation, Data curation, Conceptualization. **Stefanie Sergeant:** Resources, Methodology, Investigation, Data curation. **Quentin Smets:** Writing – review & editing, Visualization, Investigation, Formal analysis, Conceptualization. **Steven Brems:** Resources, Project administration, Funding acquisition. **Pawan Kumar:** Investigation, Formal analysis, Data curation. **Souvik Ghosh:** Investigation, Formal analysis, Data curation. **Tom Schram:** Investigation, Formal analysis, Data curation. **Sreetama Banerjee:** Investigation, Formal analysis, Data curation. **Anastasiia Kruv:** Investigation, Formal analysis, Data curation. **Dennis van Dorp:** Investigation, Formal analysis, Data curation. **Benjamin Groven:** Investigation, Formal analysis, Data curation. **Pierre Morin:** Funding acquisition, Formal analysis.

Data availability

The data that support the findings of this study are available from the corresponding author upon reasonable request.

Declaration of competing interest

The authors declare that they have no known competing financial interests or personal relationships that could have appeared to influence the work reported in this paper.

Acknowledgements

This project received funding from from the European Union's Horizon Europe Research and Innovation Program under the 2D Pilot Line (2D-PL, Grant No. 101189797).

The authors would like to acknowledge the imec programs for sample preparation and useful discussions.

References

[1] S. Wang, X. Liu, M. Xu, L. Liu, D. Yang, P. Zhou, Two-dimensional devices and integration towards the silicon lines, Nat. Mater. 21 (2022) 1225.
[2] D. Akinwande, C. Huyghebaert, C.-H. Wang, M.I. Serna, S. Goossens, L.-J. Li, H.-S. P. Wong, F.H.L. Koppens, Graphene and two-dimensional materials for silicon technology, Nature 573 (2019) 507.
[3] M.C. Lemme, D. Akinwande, C. Huyghebaert, C. Stampfer, 2D materials for future heterogeneous electronics, Nat. Commun. 13 (2022) 1392.
[4] C. Dorow, T. Schram, Q. Smets, K. O'Brien, K. Maxey, C.-C. Lin, L. Panarella, B. Kaczer, N. Arefin, A. Roy, R. Jordan, A. Oni, A. Penumatcha, C. Naylor, M. Kavrik, D. Cott, B. Groven, V. Afanasiev, P. Morin, I. Asselberghs, C.L. de la Roa, G.S. Kar, M. Metz, U. Avci, Exploring manufacturability of novel 2D channel materials: 300 mm wafer-scale 2D NMOS & PMOS using MoS_2, WS_2 & WSe_2, in: 2023 International Electron Devices Meeting (IEDM), 2023. San Francisco, USA.
[5] M. Chubarov, T.H. Choudhury, X. Zhang, J.M. Redwing, In-plane x-ray diffraction for characterization of monolayer and few-layer transition metal dichalcogenide films, Nanotechnology 29 (2018) 055706.
[6] K. Vonk, J.D. Verbakel, R. Huijink, H.J.W. Zandvliet, Sub-micrometer four-point probe transport measurements on graphene, Rev. Sci. Instrum. 94 (2023) 084707.
[7] A. Leonhardt, C.J.L. de la Rosa, T. Nuytten, L. Banszerus, S. Sergeant, V. K. Mootheri, T. Taniguchi, K. Watanabe, C. Stampfer, C. Huyghebaert, S. De Gendt, Use of the indirect photoluminescence peak as an optical probe of interface defectivity in MoS_2, Adv. Mater. Interfac. (2020) 2000413.
[8] Y. Yu, Y. Yu, C. Xu, Y.Q. Cai, L. Su, Y. Zhang, Y.W. Zhang, K. Gundogdu, L. Cao, Engineering substrate interactions for high luminescence efficiency of transition-metal dichalcogenide monolayers, Adv. Funct. Mater. 26 (2016) 4733.
[9] A. Leonhardt, T. Nuytten, C.J.L. de la Rosa, S. Sergeant, V.K. Mootheri, C. Huyghebaert, S. De Gendt, Trap density assessment of multilayer WS_2 using power-dependent indirect photoluminescence, ECS J. Solid State Sci. Technol. 9 (2020) 093016.
[10] S. Mouri, Y. Miyauchi, K. Matsuda, Tunable photoluminescence of monolayer MoS_2 via chemical doping, Nano Lett. 13 (2013) 5944.
[11] K.F. Mak, K. He, C. Lee, G.H. Lee, J. Hone, T.F. Heinz, J. Shan, Tightly bound trions in monolayer MoS_2, Nat. Mater. 12 (2013) 207.
[12] Z. Luo, H. Jia, L. Lv, Q. Wang, X. Yan, Gate-tunable trion binding energy in monolayer MoS_2 with plasmonic superlattice, Nanoscale 12 (2020) 17754.
[13] J. Pei, J. Yang, R. Xu, Y.-H. Zeng, Y.W. Myint, S. Zhang, J.-C. Zheng, Q. Qin, X. Wang, W. Jiang, Y. Lu, Exciton and trion dynamics in bilayer MoS_2, Small 11 (2015) 6384.
[14] H. Nan, Z. Wang, W. Wang, Z. Liang, Y. Lu, Q. Chen, D. He, P. Tan, F. Miao, X. Wang, J. Wang, Z. Ni, Strong photoluminescence enhancement of MoS_2 through defect engineering and oxygen bonding, ACS Nano 8 (2014) 5738.
[15] T. Korn, S. Heydrich, M. Hirmer, J. Schmutzler, C. Schüller, Low-temperature photocarrier dynamics in monolayer MoS_2, Appl. Phys. Lett. 99 (2011) 102109.
[16] J.W. Christopher, B.B. Goldberg, A.K. Swan, Long tailed trions in monolayer MoS_2: temperature dependent asymmetry and resulting red-shift of trion photoluminescence spectra, Sci. Rep. 7 (2017) 14062.
[17] C.R. Zhu, G. Wang, B.L. Liu, X. Marie, X.F. Qiao, X. Zhang, X.X. Wu, H. Fan, P. H. Tan, T. Amand, B. Urbaszek, Strain tuning of optical emission energy and polarization in monolayer and bilayer MoS_2, Phys. Rev. B 88 (R) (2013) 121301.
[18] K. Greben, S. Arora, M.G. Harats, K.I. Bolotin, Intrinsic and extrinsic defect-related excitons in TMDCs, Nano Lett. 20 (2020) 2544.
[19] S. Golovynskyi, O.I. Datsenko, D. Dong, Y. Lin, I. Irfan, B. Li, D. Lin, J. Qu, Trion binding energy variation on photoluminescence excitation energy and power during direct to indirect crossover in monolayer and few-layer MoS_2, J. Phys. Chem. C 125 (2021) 17806.
[20] S. Golovynskyi, I. Irfan, M. Bosi, L. Seravalli, O.I. Datsenko, I. Golovynska, B. Li, D. Lin, J. Qu, Exciton and trion in few-layer MoS_2: thickness- and temperature-dependent photoluminescence, Appl. Surf. Sci. 515 (2020) 146033.
[21] L. Panarella, B. Kaczer, Q. Smets, S. Tyaginov, P.S. Canflanca, A. Vici, D. Verreck, T. Schram, D. Lin, T. Knoloch, T. Grasser, C.L. de la Rosa, G.S. Kar, V. Afanas'ev, Evidence of contact-induced variability in industrially-fabricated highly-scaled MoS_2 FETs, npj 2D mater. appl. 8 (2024) 44.
[22] V. Mootheri, A. Leonhardt, D. Verreck, I. Asselberghs, C. Huyghebaert, S. De Gendt, I. Radu, D. Lin, M. Heyns, Understanding the ambipolar transport in MoS_2 field effect transistors: the substrate is the key, Nanotechnology 32 (2021) 135202.
[23] S. Ghosh, Q. Smets, S. Banerjee, T. Schram, K. Kennes, R. Verheyen, P. Kumar, M.-E. Boulon, B. Groven, H.M. Silva, S. Kundu, D. Cott, D. Lin, P. Favia, T. Nuytten, A. Phommahaxay, I. Asselberghs, C. de la Rosa, G.S. Kar, S. Brems, Integration of epitaxial monolayer MX2 channels on 300mm wafers via Collective-Die-To-Wafer (CoD2W) transfer, in: 2023 IEEE Symposium on VLSI Technology and Circuits (VLSI Technology and Circuits), 2023. Kyoto, Japan.
[24] H.M. Silva, Y. Shi, B. Groven, S. Banerjee, A.N. Mehta, I. Kandybka, A. Inoue, J. Verdin, P. Kumar, Q. Smets, S. Ghosh, D. Cott, S. Sergeant, D. Vranckx, S. Nijs, R. Verheyen, T. Schram, M.C.T. Macario, R. Rennen, F. De Groef, S. Brems, P. Morin, C. de la Rosa, I. Asselberghs, G.S. Kar, Growth of high-performance single-crystalline MoS_2 on sapphire substrates using an industrial reactor for next-

generation electronics, in: Extended Abstracts of the 2023 International Conference on Solid State Devices and Materials, vols. 6–7, 2023.
[25] C.J. McClellan, E. Yalon, K.K.H. Smithe, S.V. Suryavanshi, E. Pop, High current density in monolayer MoS_2 doped by AlO_x, ACS Nano 15 (2021) 1587.
[26] A. Leonhardt, D. Chiappe, V.V. Afanas'ev, S.E. Kazzi, I. Shlyakhov, T. Conard, A. Franquet, C. Huyghebaert, Material-selective doping of 2D TMDC through Al_xO_y encapsulation, ACS Appl. Mater. Interfaces 11 (2019) 42697.
[27] A. Rai, A. Valsaraj, H.C.P. Movva, A. Roy, E. Tutuc, L.F. Register, S.K. Banerjee, Interfacial-oxygen-vacancy mediated doping of MoS_2 by high-κ dielectrics, in: 73rd Annual Device Research Conference, 2015, pp. 189–190. Columbus, OH, USA.
[28] M. Wojdyr, Fityk: a general-purpose peak fitting program, J. Appl. Crystallogr. 43 (2010) 1126.